

A Wigner Function-Based Determinist Method for the Simulation of Quantum Transport in Silicon Nanowire Transistors

Sylvain Barraud, Thierry Poiroux, and Olivier Faynot
 CEA-Leti, Minatec campus
 17, rue des martyrs, 38054 Grenoble, Cedex 09, France
 Email: sylvain.barraud@cea.fr

Abstract—We present a model of quantum transport for Si nanowire transistor that makes use of the Wigner function formalism and takes into account carrier scattering. Scattering effects on current-voltage (I-V) characteristics are assessed using both the relaxation time approximation and the Boltzmann collision operator. Within the Fermi golden rule approximation, the standard collision term is described for both acoustic phonon and surface-roughness interactions. Then, the model is applied to study the impact of each scattering mechanism on short-channel electrical performance of Si nanowire transistors for different gate lengths.

I. INTRODUCTION

This study comes within the framework of prospective research in silicon microelectronics, which tries to take advantage of some phenomena emerging from nanoscale dimensions to continue the downscaling of MOSFET devices. Among the proposed architectures for the future technological nodes, the Si nanowires (SiNWs) have become an intensive research area over the past years. The technological advances made during the last years are accompanied by theoretical studies to determine electronic transport properties of SiNWs. Many theoretical works have been reported on low-field electron mobility calculations accounting for the electron-phonon coupling and the surface roughness based on band-structure calculated using effective-mass theory¹⁻⁴ and tight-binding methods⁵⁻⁶. However, few attempts have been reported to investigate dissipative effects in ultra-scaled SiNW-FETs because the description of scattering mechanisms at a quantum mechanical level is still computationally very challenging. The inclusion of scattering mechanisms in the Wigner formulation has been demonstrated in the case of a purely microscopic approach based on the Monte-Carlo method for the study of resonant-tunneling-diode and double-gate MOSFET⁸⁻⁹. However, the deterministic solution methods usually use phenomenological models based on the relaxation-time approximation¹⁰ (RTA). The development of such deterministic methods must also tend towards finding more realistic description of scattering terms based on Boltzmann collision operator to efficiently simulate and predict the electrical performance of 1D nanostructures such as nanowires. It is the purpose of this work to introduce phonon and surface-roughness scattering for the self-consistent study of dissipative quantum transport in gate-all-around silicon nanowires modeled with Wigner's function approach.

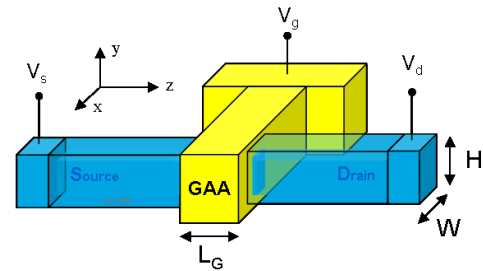


Fig. 1. Gate-all-around Si NW simulated in this work. x and y axes represent the quantization directions and the z axis represents the transport direction. W and H are the width and the height of the NW, respectively.

II. THEORY AND MODEL

The semiconductor device considered in this work is a gated silicon nanowire (Figure 1). We consider a $[001]$ -oriented SiNW with a square cross section of W in width. The wire axis is set to be the z -axis. The x and y axes represent the quantization directions. The SiNW is surrounded by 1 nm of SiO_2 oxide and a mid-gap metal gate. The device itself is between the source and drain contacts, which are assumed to be reservoirs characterized by a thermal equilibrium distribution of electrons. In order to significantly reduce the computational burden associated with computing a full 3D real-space solution, the mode-space approximation is used. Then, the nanowire is subdivided into a large number of slices along the transport direction z , and the 2D Schrödinger equation is solved in each of them. The conduction modes (or energy subbands) being determined along the transport direction, the Wigner transport equation can be solved. In 1D, the WTE is written as¹¹⁻¹³,

$$\frac{\partial f_w(z, k, t)}{\partial t} + \frac{\hbar k}{m_{eff}} \frac{\partial f_w(z, k, t)}{\partial z} + \int_{-\infty}^{+\infty} dk' f_w(z, k', t) V_w(z, k - k') = \left(\frac{\partial f_w}{\partial t} \right)_{coll} \quad (1)$$

Here $f_w(z, k, t)$ is the 1D Wigner function at position z , wavevector k and time t . The second term of the left-hand side is the kinetic term. It is exactly the same as that of the Boltzmann equation. Quantum-interference effects are

induced by the non-local potential term represented by the third term of the left-hand side. The non-local Wigner potential $V_w(z, k - k')$ is calculated from the potential energy E_ν . It is defined as⁷,

$$V_w(z, k - k') = \frac{2}{\pi\hbar} \times \int_0^{+\infty} dz' \sin[2(k - k')z'] [E_\nu(z + z') - E_\nu(z - z')] \quad (2)$$

In our application, the simulation domain is taken to be finite. The boundaries are physically given by the device contacts. Then, open boundary conditions have to be employed. The electrodes absorb outgoing particles and inject particles into the device with a Fermi-Dirac equilibrium distribution. The Wigner function being calculated, the electron density can be determined in the whole system⁷. Self-consistency is ensured with the calculation of electrostatic potential $V(x, y, z)$ satisfying 3D Poisson's equation.

III. SCATTERING IN THE WIGNER FORMULATION

In the past, the Wigner Monte-Carlo approach has been shown to provide an efficient way to study quantum transport in presence of scattering⁸⁻⁹. However, a direct solution of the steady-state Wigner transport equation has frequently been solved assuming the phenomenological relaxation time approximation for dissipative transport^{10,14-15}. In this section, additionally to the relaxation time approximation, a Boltzmann scattering operator acting on the Wigner distribution is derived for both acoustic-phonon (AP) and surface-roughness (SR) scattering mechanisms.

A. Relaxation time approximation

Similarly to the classical transport theory, the scattering mechanisms are included in the Wigner formulation through the addition of a collision term in the Liouville equation. Here, we choose to model the interactions within the RTA, which includes all dissipation processes into one macroscopic parameter. The resulting scattering term is defined as¹⁰,

$$\left(-\frac{\partial f_w}{\partial t}\right)_{coll} = -\frac{1}{\tau} \left[f(z, k) - \frac{f_{eq}(z, k)}{\int dk f_{eq}(z, k)} \int dk' f(z, k') \right] \quad (3)$$

where τ and $f_{eq}(z, k)$ denote the relaxation time and the distribution function at equilibrium, respectively. Here, $f_{eq}(z, k)$ was substituted by the equilibrium Wigner distribution function computed at $V_{DS} = 0V$. The value of τ is calculated for each conduction mode from the effective mobility through the relation $\tau = m_{eff} \times \mu/e$.

B. Boltzmann collision operator

A second approach consists in using classical scattering rates, such as are used in Monte-Carlo simulations⁸⁻⁹. Within

the Fermi golden rule approximation, the standard collision term of the Boltzmann equation may be used,

$$\left(-\frac{\partial f_w}{\partial t}\right)_{coll} = \sum_{i, k'} [P_i(k, k') f(z, k) - P_i(k', k) f(z, k')] \quad (4)$$

where i refers to the type of scattering mechanism, and $P_i(k, k')$ is the 1D transition probability from state k to state k' . The scattering rates due to acoustic phonons and surface-roughness interactions are computed using the deformation potential approximation usually used in the framework of the effective mass.

1) *Acoustic phonon scattering*: Here, bulk phonons are considered and the interaction is assumed to be elastic. The transition probability, calculated using the Fermi golden rule, can be written as³⁻⁴

$$P(k) = \sum_{\nu'} \frac{2\Xi_{ac}^2 k_B T \sqrt{2m_{eff}}}{\rho \hbar^2 v_s^2} D_{\nu\nu'}^{\eta\eta} \frac{\Theta[E_{\eta,\nu}(k) - E_{\eta,\nu'}]}{\sqrt{E_{\eta,\nu}(k) - E_{\eta,\nu'}}} \frac{1 + 2\alpha_\eta[E_{\eta,\nu}(k) - E_{\eta,\nu'}]}{\sqrt{1 + \alpha_\eta[E_{\eta,\nu}(k) - E_{\eta,\nu'}]}} \quad (5)$$

where

$$D_{\nu\nu'}^{\eta\eta} = \iint dx dy |\varphi_{\eta,\nu}(x, y)|^2 |\varphi_{\eta,\nu'}(x, y)|^2 \quad (6)$$

$D_{\nu\nu'}^{\eta\eta}$ represents the overlap integral between wavefunction $|\varphi_{\eta,\nu}(x, y)|$ of subband ν related to the valley η and wavefunction $|\varphi_{\eta,\nu'}(x, y)|$ of subband ν' related to the same valley. Ξ_{ac} is the acoustic deformation potential, $\rho = 2.3 \times 10^3 \text{ kg.m}^{-3}$ is the crystal density, $v_s = 9 \times 10^3 \text{ m.s}^{-1}$ is the sound velocity, m_{eff} is the effective mass, Θ is the Heaviside step function, k_B is the Boltzmann constant, $\alpha_n = 0.5 \text{ eV}^{-1}$ is the nonparabolicity factor, and T is the temperature.

2) *Surface roughness scattering*: The surface roughness is described by two parameters - the root-mean-square deviation Δ and the correlation length Λ . It is assumed that surface roughness scattering induces only intravalley transitions and that the four interfaces are uncorrelated. In the present work, we give only the derivation of the matrix element for the surface roughness at the top interface. The matrix element associated to the surface roughness at other interfaces can be obtained in a similar way.

The scattering rate due to the surface roughness can be expressed as³⁻⁴,

$$P(k) = \sum_{\nu'} \frac{\sqrt{2m_{eff}}}{\hbar^2} \frac{\sqrt{2}\Delta^2\Lambda}{2 + q_z^2\Lambda^2} |\Gamma_{\eta\nu\nu'}^{GPN}|^2 \frac{\Theta[E_{\eta,\nu}(k) - E_{\eta,\nu'}]}{\sqrt{E_{\eta,\nu}(k) - E_{\eta,\nu'}}} \frac{1 + 2\alpha_\eta[E_{\eta,\nu}(k) - E_{\eta,\nu'}]}{\sqrt{1 + \alpha_\eta[E_{\eta,\nu}(k) - E_{\eta,\nu'}]}} \quad (7)$$

with $q_z = k_z \pm k'_z$ the difference between the initial (k_z) and the final (k'_z) electron wavevectors and the top (bottom) sign is for backward (forward) scattering. $\Gamma_{\eta\nu\nu'}^{GPN}$ represents the generalized Prange-Nee term expressed as³⁻⁴,

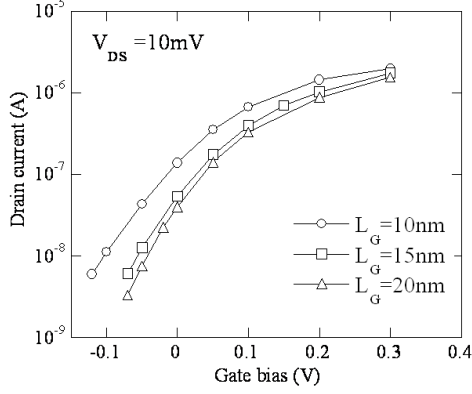


Fig. 2. $I_{DS} - V_{GS}$ characteristics calculated in the ballistic regime for a drain voltage $V_{DS} = 10mV$. The square cross-section is $5 \times 5nm^2$ and the channel length varies from $L_c = 20nm$ down to $10nm$.

$$\Gamma_{\eta\nu\eta'\nu'}^{GPN} = -\frac{\hbar^2}{W} \int_0^W dx \int_0^W dy \varphi_{\eta,\nu} \left[\frac{\partial}{\partial y} \frac{1}{m_{\eta,y}^{eff}} \frac{\partial \varphi_{\eta,\nu'}}{\partial y} \right] + \int_0^W dx \int_0^W dy \varphi_{\eta,\nu} \left(1 - \frac{y}{W} \right) \frac{\partial V}{\partial y} \varphi_{\eta,\nu'} + (E_{\eta,\nu} - E_{\eta,\nu'}) \times \int_0^W dx \int_0^W dy \varphi_{\eta,\nu} \left(1 - \frac{y}{W} \right) \frac{\partial \varphi_{\eta,\nu'}}{\partial y}. \quad (8)$$

It is composed of three terms which correspond to the fluctuations of wave functions, electrostatic potential and energy levels induced by the surface roughness, respectively.

IV. RESULTS AND DISCUSSION

A. Ballistic quantum transport

For the *gate-all-around* Si nanowire transistor represented in Figure 1, with a width of $5nm$, the $I_{DS} - V_{GS}$ characteristics calculated at $V_{DS} = 0.01V$ and for different gate lengths are shown in Figure 2. An example of Wigner's function resulting from the solution of the Liouville equation is also illustrated in Figure 3. In the highly doped source-drain extensions, a Maxwell-Boltzmann distribution function is recovered. However, in the channel, oscillations of Wigner's function induced by the non-local potential are clearly observed.

B. Relaxation time approximation

To go further into the electronic transport description, the RTA is used to consider scattering effects¹⁰. In Figure 4, we present the transfer characteristics $I_{DS} - V_{GS}$ calculated in the ballistic regime and using the momentum relaxation time for including the collision term. Here, two mobility values ($\mu = 96cm^2/Vs$ and $386cm^2/Vs$) are used in the drain current calculation. It appears that a reduction of electron mobility is logically accompanied by a drain current degradation. By varying the mobility down to $96cm^2/Vs$, a current reduction of 71% is obtained. The current reduction is defined as $(I_{bal} - I_{scatt})/I_{bal}$, with I_{bal} and I_{scatt} the ballistic and the dissipative currents, respectively. Since interactions cause the electron distribution to approach $f_{eq}(z, k)$, one may expect

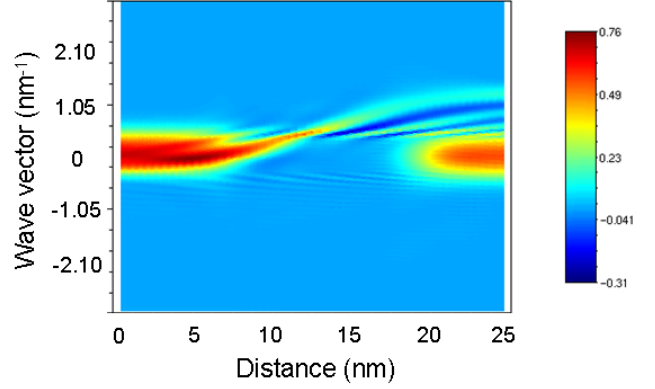


Fig. 3. Cartography of the Wigner function related to the first energy subband for $V_{GS} = 0.2V$ and $V_{DS} = 0.3V$. The channel length is $L_c = 10nm$ and the square cross-section is $5 \times 5nm^2$.

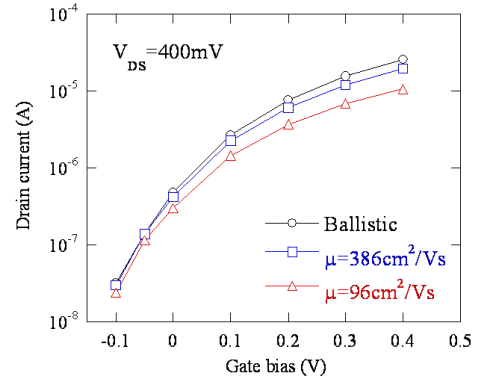


Fig. 4. $I_{DS} - V_{GS}$ characteristics calculated in the ballistic regime and using the momentum relaxation time for including the collision term. The channel length is $L_c = 10nm$, the square cross-section is $5 \times 5nm^2$ and $V_{DS} = 0.4V$.

that the severe quantum oscillations in the Wigner function (Cf. Fig. 3) will tend to be degraded in the case of dissipative transport. Indeed, the Figure 5 reports the cartography of the Wigner function (only for positive wave vector) related to the first energy subband. The Wigner function is represented in the case of ballistic transport, and using the momentum relaxation time approximation with $\mu = 386cm^2/Vs$ and $\mu = 96cm^2/Vs$. It is apparent that the oscillations are diminished greatly by comparison to the collisionless case, and that for high relaxation time, the oscillations are almost completely destroyed.

C. Boltzmann collision operator

Let us now concentrate on the calculation of the transition rates needed to obtain the Wigner distribution function by using the Boltzmann collision operator. Here, both AP and SR scattering rates are accounted for. An acoustic deformation potential of $11eV$ is used for silicon. The surface roughness is defined with $\Delta = 0.3nm$ and $\Lambda = 1.3nm$. It has been previously demonstrated that these parameters are well

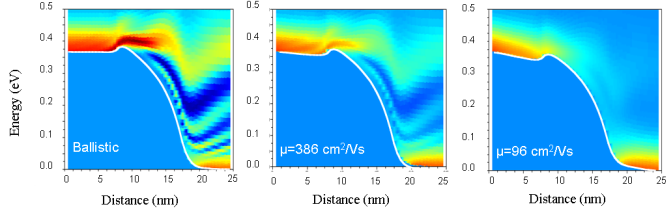


Fig. 5. Cartography of the Wigner function (only for positive wave vector) related to the first energy subband for $V_{GS} = 0.3V$ and $V_{DS} = 0.4V$. The channel length is $L_c = 10nm$ and the square cross-section is $5 \times 5nm^2$. The Wigner function is represented in the case of ballistic transport and using the momentum relaxation time with $\mu = 386cm^2/Vs$ and $96cm^2/Vs$.

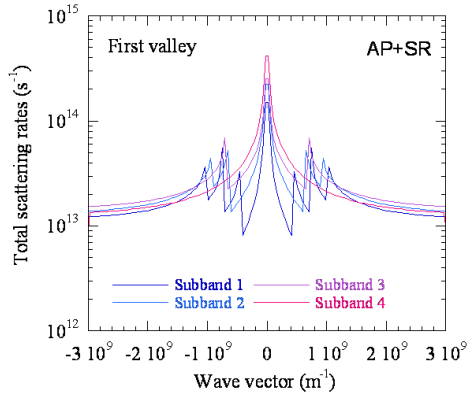


Fig. 6. Calculation of acoustic phonon (AP) and surface-roughness (SR) scattering rates. The total scattering rate is extracted in the source of SiNW with $L_c = 10nm$, $W = 5nm$, $V_{GS} = 0.3V$, and $V_{DS} = 0.01V$.

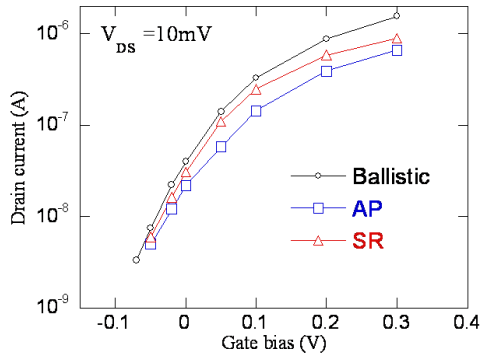


Fig. 7. $I_{DS} - V_{GS}$ characteristics calculated in the ballistic regime and with AP and SR scattering. The channel length is $L_c = 20nm$, the square cross-section is $5 \times 5nm^2$, and $V_{DS} = 0.01V$.

suites to accurately reproduce the mobility curves in SiNW transistors⁴. In contrast to the RTA, intersubband transitions are accounting for. In Figure 6, the calculation of AP and SR scattering rates for the first four energy subband is reported as a function of the wavevector. In Figure 7 we show the $I_{DS} - V_{GS}$ curves calculated in the ballistic regime and using the Boltzmann collision operator. A drain current reduction of 57% is observed due to the AP scattering against 43% for the SR scattering at $V_{GS} = 0.3V$ and $V_{DS} = 0.01V$ (Figure 8).

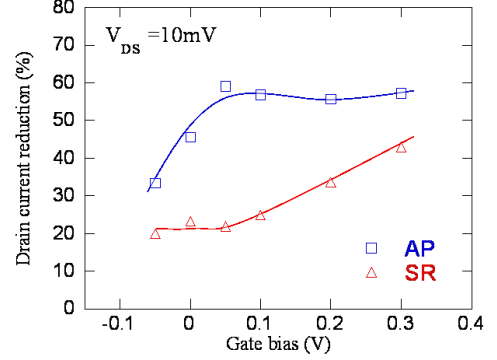


Fig. 8. Drain current reduction due to AP and SR scattering at $V_{DS} = 0.01V$ as a function of V_{GS} .

V. CONCLUSION

An efficient numerical model for the simulation of dissipative quantum transport in nanoscale SiNW transistors is presented. The model is based on a direct solution of 1D WTE coupled with a 2D Schrödinger/3D Poisson algorithm. Scattering effects on the current-voltage characteristics are modeled using Boltzmann collision operator with the calculation of phonon and surface-roughness scattering in each slice of the NW along the transport direction. This model allows to identify the different mechanisms limiting the transport in short-channel MOSFET devices. It can be used to evaluate the role played by each interaction on electrical performance of NWFETs for different gate lengths and NW widths.

ACKNOWLEDGMENT

This work is partially funded by the IBM-STMicroelectronics-CEA/LETI-MINATEC Development Alliance. It was performed using HPC resources at CCRT and CINES made available by GENCI under grant 2011096666.

REFERENCES

- [1] R. Kotlyar, B. Obradovic, P. Matagne, M. Stettler, and M.D. Giles, *Appl. Phys. Lett.* **84**, 5270 (2004).
- [2] S. Jin, M.V. Fischetti, and T. Tang, *J. Appl. Phys.* **102**, 083715 (2007).
- [3] E.B. Ramayya, D. Vasileska, S.M. Goodnick, and I. Knezevic, *J. Appl. Phys.* **104**, 063711 (2008).
- [4] S. Barraud, E. Sarrazin, and A. Bournel, *Semicond. Sci. Technol.* **26**, 025001 (2011).
- [5] W. Zhang, C. Delerue, Y.-M. Niquet, G. Allan, and E. Wang, *Phys. Rev. B* **82**, 115319 (2010).
- [6] M. Luisier, *Appl. Phys. Lett.* **98**, 032111 (2011).
- [7] S. Barraud, *J. Appl. Phys.* **106**, 063714 (2009).
- [8] N. Nedjalkov, H. Kosina, S. Selberherr, C. Ringhofer, and D.K. Ferry, *Phys. Rev. B* **70**, 115319 (2004).
- [9] D. Querlioz, H.-N. Nguyen, J. Saint-Martin, A. Bournel, S. Galdin-retailleau, and P. Dollfus, *J. Comput Electron* **8**, 324 (2009).
- [10] Y. Yamada, H. Tsuchiya, and T. Miyoshi, *IEEE Trans. Electron. Devices* **56**, 1396 (2009).
- [11] W.R. Frensley, *Rev. Mod. Phys.* **62**, 745 (1990).
- [12] C. Jacoboni, and P. Bordone, *Rep. Prog. Phys.* **67**, 1033 (2004).
- [13] H. Kosina, M. Nedjalkov, *Handbook of Theoretical and Computational Nanotechnology* **10**, 731 (2006).
- [14] N.C. Klusdahl, A.M. Kriman, and D.K. Ferry, *Phys. Rev. B* **39**, 7720 (1989).
- [15] Z. Dai and J. Ni, *Eur. Phys. J. B.* **45**, 129 (2005).
- [16] S.M. Goodnick, D.K. Ferry, C.W. Wilmsen, Z. Liliental, D. Fathy, and O.L. Krivanek, *Phys. Rev. B* **12**, 2265 (1975).